Microwave imaging reflectometry for the visualization of turbulence in tokamaks

E. Mazzucato

Princeton Plasma Physics Laboratory, Princeton University,
Princeton, New Jersey, United States of America

Abstract. Understanding the mechanism of anomalous transport in magnetically confined plasmas requires the use of sophisticated diagnostic tools for the measurement of turbulent fluctuations. The article describes the results of an extensive numerical study of microwave reflectometry in tokamaks showing that the two dimensional structure of plasma fluctuations near the cut-off can be obtained from the phase of reflected waves. This requires the latter to be collected by an optical system making an image of the reflecting layer onto an array of microwave receivers, and the amplitude of fluctuations to be below a threshold that is set by the spectrum of poloidal wavenumbers. The conceptual design of an experimental scheme for the global visualization of turbulent fluctuations in tokamaks is described.

1. Introduction

The direct impact of plasma confinement on the feasibility of an economical fusion reactor makes understanding the mechanism of anomalous transport in magnetically confined plasmas one of the great challenges of fusion research.

Both theory and experiments suggest that plasma transport in tokamaks exceeds the neoclassical predictions because of the existence of a short scale turbulence causing an enhancement in the diffusion of particles, energy and momentum across the magnetic field lines [1]. However, such an explanation is not completely satisfactory since it is based neither on a self-consistent theory of plasma turbulence nor on a comprehensive set of measurements. Indeed, the role played by turbulence in the transport of magnetically confined plasmas is still an outstanding issue.

Because of the overwhelming difficulty in developing a theory of plasma turbulence and in performing exhaustive measurements of short scale fluctuations, numerical simulations are beginning to play a dominant role in the prediction and interpretation of tokamak experiments. However, this is also not satisfactory since, given the enormous complexity of the problem, any simulation of turbulence must be driven by a direct experimental observation of turbulent fluctuations. A case in point is that of classical fluids [2], where many advances in the theory of hydrodynamic turbulence were stimulated by the visualization of the turbulent flow with a variety of optical techniques. Unfortunately, none of these diagnostic methods can be used for the measurement of fluctuations in low density and high temperature plasmas, such as those in tokamaks.

In this article, a method for the global visualization of turbulent fluctuations in tokamaks is described. The outline is as follows. In Section 2, a discussion is given of the difficulties and limitations in the use of standard microwave reflectometry. Section 3 contains results from a series of numerical simulations, and their implications for the use of reflectometry in tokamaks are discussed in Section 4. Section 5 describes the conceptual design of a possible apparatus for the global visualization of turbulent fluctuations in tokamaks. Finally, the conclusions are presented in Section 6.

2. Microwave reflectometry

The method described in this article is based on microwave reflectometry [3] — a radar technique for the detection of plasma fluctuations from the reflection of microwaves by a plasma cut-off. Because of a high sensitivity to plasma fluctuations, this method has found extensive use in tokamaks for the detection of turbulence. However, as we shall see in the following, very often the high sensitivity makes the extraction of any quantitative information from the measured signals very difficult as well.

The interpretation of reflectometry is relatively simple in a 1-D geometry, where a plane stratified plasma permittivity $\varepsilon = \varepsilon_0(r) + \tilde{\varepsilon}(r)$ (with fluctuation component $\tilde{\varepsilon}(r) \ll 1$) is probed by a wave propagating in the r direction. Under these conditions, it is easy to show that when the radial wavenumber of fluctuations satisfies the equation $k_r < k_0/(k_0 L_\varepsilon)^{1/3}$ (where $L_\varepsilon = (d\varepsilon_0/dr)^{-1}_{r=r_c}$ is the scale length of the

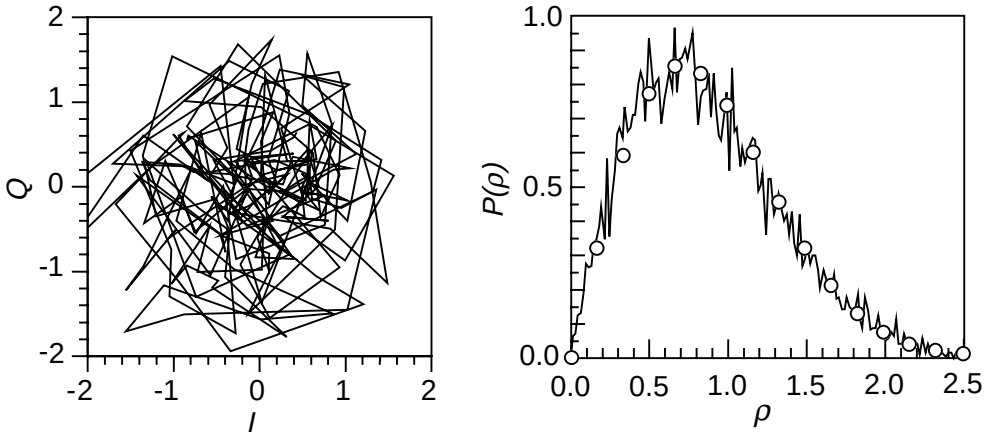

Figure 1. In-phase (I) and quadrature (Q) components of a TFTR reflectometer signal in a 200 μs window (left), and probability density distribution of the signal amplitude $\rho = \sqrt{I^2 + Q^2}$ (right); open circles are the Rayleigh distribution ($2\rho \exp[-\rho^2]$).

plasma permittivity at the cut-off $r = r_c$, and k_0 is the free-space wavenumber of the probing beam), the fluctuating component of the signal phase is given by the approximation of geometric optics [3]

$$\tilde{\phi} = k_0 \int_0^{r_c} \frac{\tilde{\varepsilon}(r)}{\sqrt{\varepsilon_0(r)}}\, dr. \qquad (1)$$

By taking $|k_r| > 1/L_\varepsilon$, since we are interested in short scale fluctuations, and $\varepsilon_0(r) \approx (r_c - r)/L_\varepsilon$, since most of the contribution to $\tilde{\phi}$ comes from a narrow region near the cut-off, from Eq. (1) we obtain [3]

$$\Gamma_\phi(k_r) = \pi M \frac{k_0^2 L_n}{|k_r|} \Gamma_n(k_r) \qquad (2)$$

where $L_n = n/(dn/dr)_{r=r_c}$ is the scale length of the electron density n, $M \equiv (n\partial\varepsilon/\partial n)_{r=r_c}$ (≈ 1 for the ordinary mode and ≈ 2 for the extraordinary mode), $\Gamma_\phi(k_r)$ is the power spectrum of $\tilde{\phi}$ (considered as a function of r_c) and $\Gamma_n(k_r)$ is the power spectrum of the relative plasma density fluctuation $\tilde{n}/n$.

In conclusion, for a 1-D turbulence, the power spectrum of density fluctuations ($\Gamma_n(k_r)$) can be obtained from the power spectrum of the signal phase ($\Gamma_\phi(k_r)$). The latter can be measured by performing radial correlation measurements using several probing waves with closely spaced cut-off layers.

The use of reflectometry becomes considerably more difficult in plasmas with multidimensional turbulent fluctuations. Unfortunately, this is just the case of interest in magnetically confined plasmas, such as in tokamaks, where turbulent fluctuations vary in both radial and poloidal directions. The difficulty stems from the fact that, when the plasma permittivity fluctuates perpendicularly to the direction of propagation of the probing wave, the spectral components of the backward field propagate along different directions. This may result in a complicated interference pattern on the detector plane, from which it is very difficult to extract any information on the fluctuations under investigation. This phenomenon is illustrated in Fig. 1, which shows the in-phase (I) and the quadrature (Q) components of a TFTR reflectometer signal together with the density distribution of the amplitude $\rho = \sqrt{I^2 + Q^2}$ [4]. The fluctuations in the amplitude of the measured signal are the result of large 2-D plasma density fluctuations that transform the signal components into two independent normal random variables with zero mean, as demonstrated in Fig. 1 by the random walk of the complex amplitude (left) and the Rayleigh distribution of ρ (right). Consequently, this is a case where the measured signals cannot be used for inferring the properties of plasma fluctuations.

To better understand and quantify this phenomenon, we have performed a series of numerical simulations of reflectometry in plasmas with 2-D fluctuations [5]. Here we will present only the results that are of interest for the subject of this article.

3. Numerical simulations

In a system of orthogonal co-ordinates (x, r), we assume that a plane stratified plasma density ($n(r)$)

is perturbed by a field of 2-D fluctuations ($\tilde{n}(x,r)$) with spectral distribution

$$\frac{\tilde{n}(x,r)}{n(r)} = \sum_{p=1}^{M}\sum_{q=1}^{M} \Delta_{pq} \cos(p\kappa_r r)\cos(q\kappa_x x + \varphi_{pq}) \quad (3)$$

consisting of $M \times M$ discrete components with wavenumbers $p\kappa_r$ and $q\kappa_x$ (κ_r and κ_x are constants), random phases φ_{pq} and amplitudes

$$\Delta_{pq}^2 \propto p \exp[-(p\kappa_r/\Delta k_r)^2 - (q\kappa_x/\Delta k_x)^2] \quad (4)$$

where $\Delta k_r = \kappa_r M/2$ and $\Delta k_x = \kappa_x M/2$. Throughout this article we will use the value $M = 20$.

The plasma is confined to the region $r < r_b$, and the probing wave is launched in the r direction from the free-space region $r > r_b$. For facilitating the comparison with experimental results, the density $n(r)$ is taken similar to the electron density distribution on the equatorial plane of a typical TFTR discharge. Finally, the probing wave has a frequency of 75 GHz and the ordinary mode of propagation with the electric field perpendicular to the x axis.

The wave amplitude ($E(x,r)$) is expressed as the sum of $2N+1$ independent solutions of the wave equation

$$E(x,r) = \sum_{n=-N}^{N} c_n E_n(x,r) \quad (5)$$

where $N \gg M$ (to be determined). The functions E_n are cast in the form

$$E_n(x,r) = \sum_{m=-N}^{N} f_{mn}(r) e^{im\kappa_x x} \quad (6)$$

where $f_{mn}(r)$ are solutions of the system of $2N+1$ ordinary differential equations

$$\frac{d^2 f_{mn}}{dr^2} + k_0^2(\varepsilon_0 - \alpha_m^2) f_{mn} + k_0^2(\varepsilon_0 - 1) \times \sum_{p=1}^{M}\sum_{q=1}^{M} \left[\frac{\Delta_{pq}}{2} \cos(p\kappa_r r)(f_{(m-q)n} e^{i\varphi_{pq}} + f_{(m+q)n} e^{-i\varphi_{pq}}) \right] = 0 \quad (7)$$

$(m = -N,\ -N+1,...,N)$

with $\varepsilon_0 = 1 - (\omega_p/\omega)^2$ the unperturbed permittivity, $\omega_p = (4\pi n_e e^2/m_e)^{1/2}$ the plasma frequency and $\alpha_m = m\kappa_x/k_0$. These equations, which are obtained by inserting Eqs (3) and (6) into the wave equation and performing a Fourier expansion in x, can be solved with the Runge–Kutta method. The coefficients c_n in Eq. (5) are obtained by imposing on the wave amplitude in free space the form

$$E(x,r) = e^{-ik_0 r} + \sum_{n=-N}^{N} A_n e^{i[n\kappa_x x + (k_0^2 - n^2\kappa_x^2)^{1/2} r]} \quad (8)$$

where the first term on the right hand side is the launched wave, while the second represents the field of reflected waves (in the following referred to as the backward field E_b). In the region $r < r_b$, E_b represents a virtual field that an observer in free space could measure by mapping the plasma region onto an array of detectors using an optical system.

Finally, the integer N must be chosen large enough to make the results significantly unchanged by any increase in its value. This condition, to be verified a posteriori, allows the closure of the system of differential equations (7) by setting to zero all terms $f_{(m\pm q)n}$ with $|m \pm q| > N$.

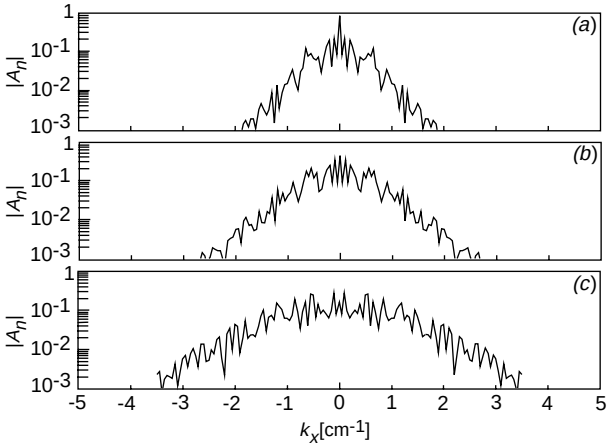

Figure 2. Spectra of backward waves in free space as a function of k_x for fluctuations with $\Delta k_x = 0.5$ cm^{-1}, $\Delta k_r = 1$ cm^{-1} and $\sigma_n = 2.5 \times 10^{-3}$ (a), $\sigma_n = 5.0 \times 10^{-3}$ (b), $\sigma_n = 1.0 \times 10^{-2}$ (c). Calculations were done with $N = 80$.

Shown in Fig. 2 are the amplitudes $|A_n|$ of reflected waves as a function of $k_x = n\kappa_x$ for fluctuations with $\Delta k_x = 0.5$ cm^{-1} and $\Delta k_r = 1$ cm^{-1}. The three cases shown in Fig. 2 differ only in the value of the total density fluctuation (defined as the volume average $\sigma_n = \langle \tilde{n}^2/n^2 \rangle^{1/2}$), which is equal to 2.5×10^{-3}, 5.0×10^{-3} and 1.0×10^{-2}, respectively. These results show that a rise in the level of plasma fluctuations causes a spectral broadening of the reflected waves, and a decrease in the amplitude

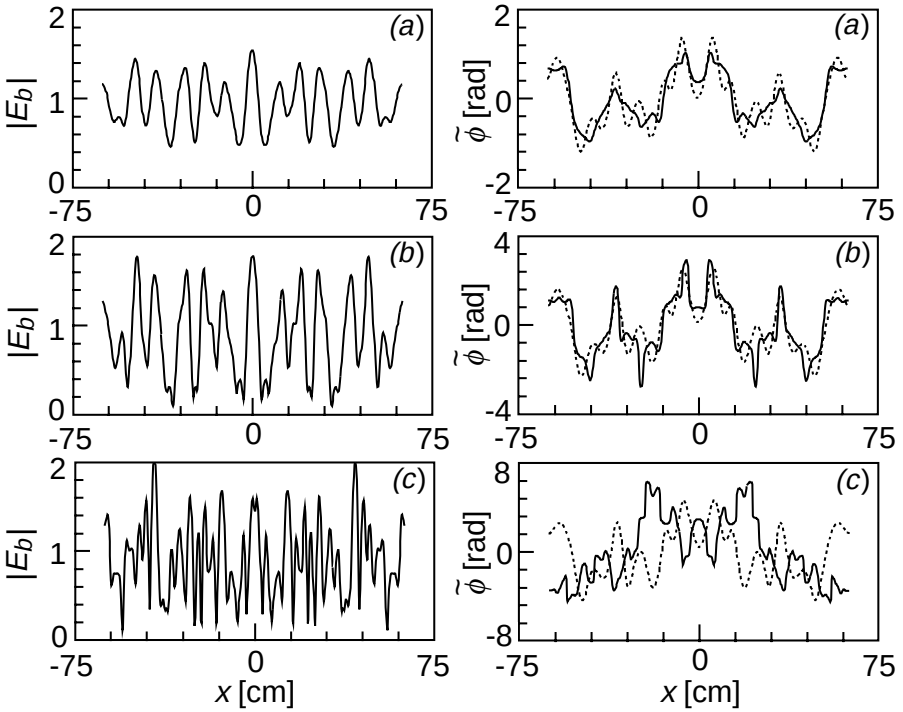

Figure 3. Modulus of the backward field $|E_b|$ (left) and fluctuating phase $\tilde{\phi}$ (right) at the plasma boundary ($r = r_b$) for the three cases of Fig. 2. The dashed line is the phase of 1-D geometric optics (ϕ_{GO}).

(A_0) of the wave propagating along the direction of the specular reflection ($k_x = 0$).

For the three cases of Fig. 2, the modulus ($\rho = |E_b|$) and the phase deviation ($\tilde{\phi}$) from the mean of the backward field at the plasma boundary ($r = r_b$) are shown in Fig. 3. The large fluctuations in ρ indicate that the backward field is far from being a plane wave. Also shown in Fig. 3 is the phase obtained from Eq. (1) neglecting the bending of rays, which in the following we will indicate with ϕ_{GO} and refer to as the phase of 1-D geometric optics. These results show that $\tilde{\phi}$ is significantly different from ϕ_{GO}, and that the discrepancy grows with the level of plasma fluctuations.

In Fig. 3, similarly to the experimental case in Fig. 1, large variations in ρ are caused by the interference of reflected waves. The question, then, is whether the fluctuations in ρ are smaller at other radial locations. According to the random phase screen model of reflectometry [6], where the primary effect of plasma fluctuations is assumed to be a phase modulation of the probing wave near $r \approx r_c$, these fluctuations should be very small near the cut-off region.

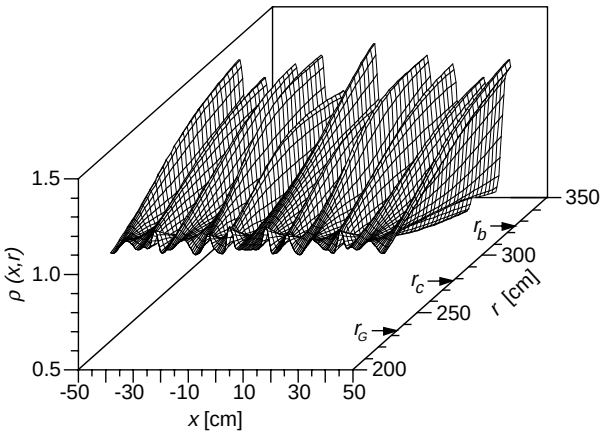

Figure 4. Isometric 3-D plot of the field amplitude $\rho(x, r)$ for case (a) of Fig. 2; the probing wave is launched from the free-space region $r > r_b$.

The isometric 3-D plot of Fig. 4 shows that a region with small variations in $\rho(x, r)$ indeed exists. However, such a region is located at a considerable distance from the cut-off. As a measure of the fluctuation in the amplitude of the backward field, we define the variance $\sigma_\rho^2(r) = \langle(\rho - \langle\rho\rangle_r)^2\rangle_r$, where

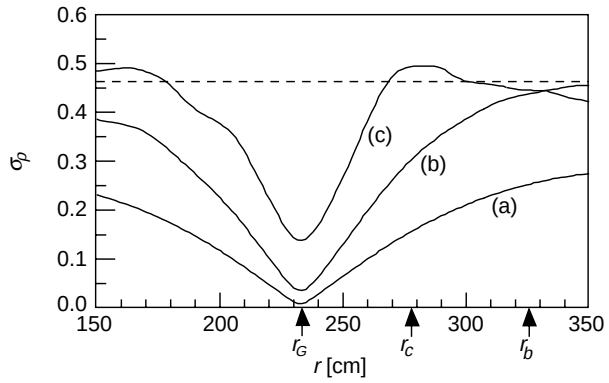

Figure 5. Value of σ_ρ as a function of r for the three cases of Fig. 2. The dashed line represents the value of σ_ρ from the Rayleigh distribution.

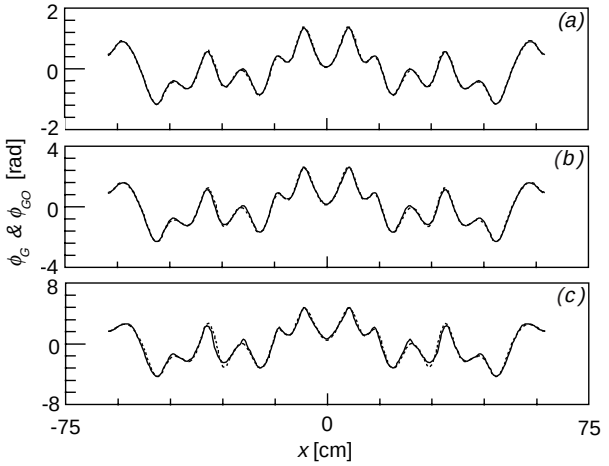

Figure 6. Fluctuating phases ϕ_G (solid line) and ϕ_{GO} (dashed line) for the cases of Fig. 2.

$\langle ... \rangle_r$ indicates the average at a constant value of r. Figure 5 shows that in all three cases of Fig. 2 the absolute minimum of σ_ρ occurs at the same radius $r = r_G$.

It is also interesting to note that for $r \gg r_G$, σ_ρ approaches the variance given by the Rayleigh distribution of a Gaussian noise, indicating that, as in Fig. 1, the real and the imaginary components of the backward field become two independent normal random variables with zero mean.

Shown in Fig. 6 is the value of ϕ_{GO} and the phase deviation from the mean of the backward field at $r = r_G$ (in the following referred to as the phase ϕ_G). The excellent agreement between ϕ_{GO} and ϕ_G is tantamount to a reduction of the problem of 2-D fluctuations to that of 1-D fluctuations. In both cases, Eq. (2) provides a link between the plasma

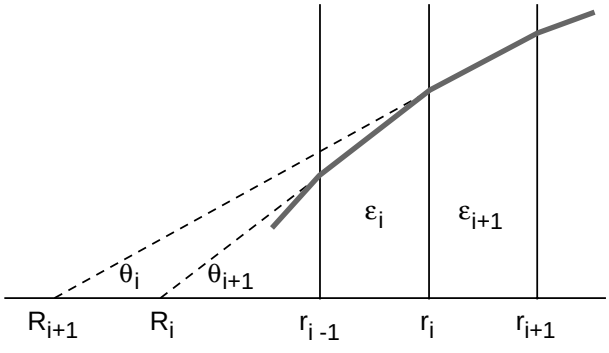

Figure 7. Geometry used for deriving Eq. (9).

fluctuations and a measurable phase — the phase of measured signals for 1-D fluctuations and the phase ϕ_G for 2-D fluctuations.

These properties of the plane $r = r_G$, i.e. where σ_ρ is minimum and $\phi_G \approx \phi_{GO}$, would make the backward field appear to an observer in free space as coming from a virtual location behind the cut-off. This is caused by the spatial variation of ε_0 that produces a bending towards the r axis in the trajectory of waves with $k_x \neq 0$. To quantify this phenomenon, let us consider the geometry of Fig. 7, where the plasma is divided into N plane slabs with thickness δ and uniform permittivity ε_i. For a ray with wavenumber k_x, we can easily derive the difference equation

$$l_{i+1} - l_i = l_i \frac{\tan(\theta_i)}{\tan(\theta_{i+1})} - l_i + \delta \tag{9}$$

where R_i and θ_i are the radius and the angle of intersection with the r axis of the ray tangent, and $l_i = r_i - R_i$.

From this and the fact that k_x is constant, we obtain

$$\frac{l_{i+1} - l_i}{\delta} \approx \frac{l_i}{\sqrt{\varepsilon_i - \alpha}} \frac{\sqrt{\varepsilon_{i+1} - \alpha} - \sqrt{\varepsilon_i - \alpha}}{\delta} + 1 \tag{10}$$

where $\alpha = (k_x/k_0)^2$. The limit $N \to \infty$ turns Eq. (10) into the differential equation

$$\frac{d}{dr} \frac{l(r)}{\sqrt{\varepsilon_0(r) - \alpha}} = \frac{1}{\sqrt{\varepsilon_0(r) - \alpha}} \tag{11}$$

which, apart from terms of order αL_ε, gives

$$l(r = r_b) \approx \int_{r_c}^{r_b} \frac{1}{\sqrt{\varepsilon_0(r)}} dr. \tag{12}$$

Since this expression does not depend on k_x, all rays starting from the same point would appear in free space as coming from the radial position

$$r = r_G \approx r_b - \int_{r_c}^{r_b} \frac{1}{\sqrt{\varepsilon_0(r)}} dr. \tag{13}$$

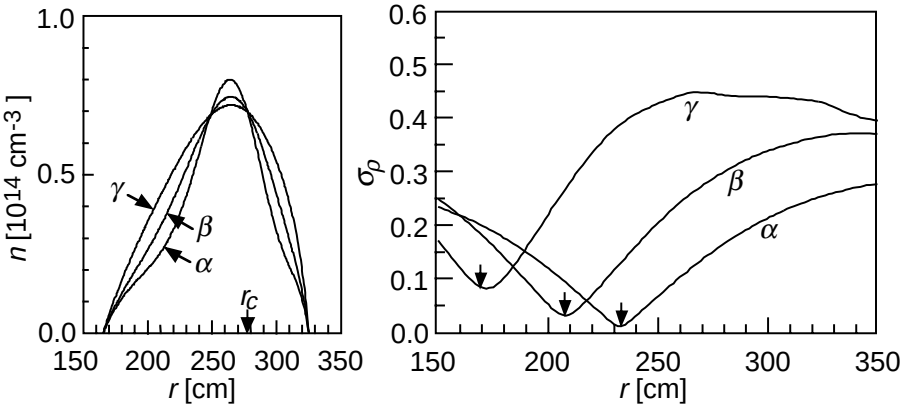

Figure 8. Value of σ_ρ (right) for three density profiles (left) with identical cut-offs (α is the profile used throughout this article). Plasma fluctuations are as in case (a) of Fig. 2. Arrows on right graph indicate the value of r_G from Eq. (13).

It is interesting to note that the integral in this equation is the group delay multiplied by the speed of light. The results in Fig. 8, where $\sigma_\rho(r)$ is displayed for three density profiles with identical cut-offs, show that Eq. (13) agrees with the results of the numerical simulations.

In deriving Eq. (13) we have neglected terms of order $L_\varepsilon(k_x/k_0)^2$, which is the order of magnitude of the displacement from the cut-off of the turning points of backward waves. Since these terms depend on k_x, their inclusion would make r_G depend on k_x as well. This explains why the minimum value of σ_ρ increases with both σ_n (as in Fig. 5) and L_ε (as in Fig. 8), since the range of k_x of the backward waves increases in both cases. As we shall see in Section 4, this sets the conditions for the applicability of the method proposed in this article.

The results described so far represent an enormous reduction in the difficulty of obtaining the spectrum of turbulent fluctuations from reflectometry data. However, as explained in the introduction, we are looking for an experimental technique capable of providing a direct visualization of turbulent fluctuations. Thus the crucial issue is the similarity of the phase ϕ_G to the local value of density fluctuations near the cut-off. This is illustrated in Fig. 9, again for the three cases of Fig. 2, showing the phase ϕ_G and the normalized plasma density fluctuation $n^* \equiv (\sigma_\phi/\sigma_n)(\tilde{n}/n)$ (where the normalizing coefficient $\sigma_\phi/\sigma_n = (\pi^{3/2}k_0^2 L_n/\Delta k_r)^{1/2}$ is obtained from Eqs (2)–(4)). The radius in Fig. 9 is $r = r_c + 0.8$ cm, which is the value giving the best agreement between n^* and ϕ_G. This radial position is

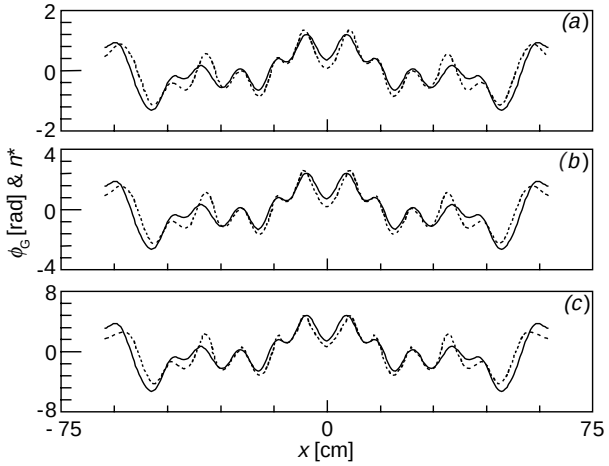

Figure 9. Phase ϕ_G (dashed line) and normalized density fluctuation n^* at $r = r_c + 0.8$ cm (solid line) for the three cases of Fig. 2.

shifted from r_c by an amount of order $(k_0 L_\varepsilon)^{1/3}/k_0$, i.e. it is located where the amplitude of waves with $|k_x| \ll k_0$ (approximately an Airy function) is the largest. The small discrepancy between ϕ_G and n^* can be explained by the different structure of these two quantities, the former being an integral function of the latter. This is also what causes the different dependence on k_r of the two power spectra in Eq. (2).

The similarity between n^* and ϕ_G degrades very quickly moving away from the radial position giving the best agreement. This is illustrated in Fig. 10, which shows ϕ_G and n^* at three radial locations for plasma fluctuations similar to those of case (b) in Fig. 2, but with a larger value of $\Delta k_r = 2.0$ cm^{-1}

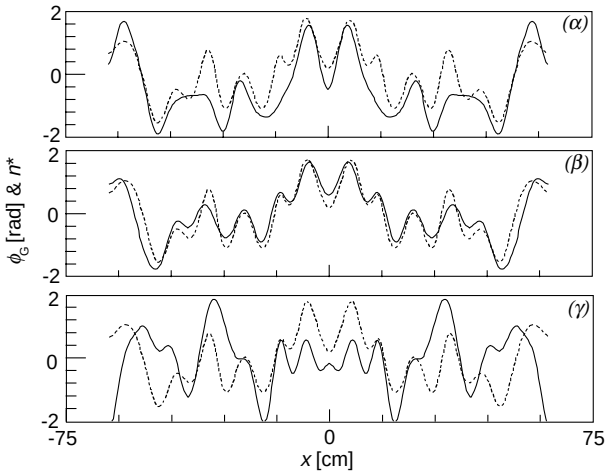

Figure 10. Phase ϕ_G (dashed line) and normalized density fluctuations n^* (solid line) for $r = r_c$ (α), $r = r_c + 0.8$ cm (β) and $r = r_c + 1.8$ cm (γ). Fluctuations are as in case (b) of Fig. 2 but with $\Delta k_r = 2$ cm^{-1}.

(corresponding to a radial correlation length of ∼1 cm). Note that the radial position where the discrepancy between ϕ_G and n^* is minimum is again at $r = r_c + 0.8$ cm, where, in spite of the shorter scale of fluctuations, it is almost identical to that displayed in Fig. 9. Thus the conclusion is that the measurement of the phase ϕ_G can provide the local value of the plasma density fluctuation near the cut-off.

4. Discussion

The results in the previous section can be summarized by saying that the field of reflected waves arises near the cut-off from the phase modulation of the probing wave, with a magnitude given by 1-D geometric optics, i.e. neglecting the effects of fluctuations on ray trajectories. Because of the distortion caused by the non-uniformity of the average plasma permittivity (ε_0), the backward field appears to arrive from a distant point behind the cut-off ($r = r_G$), where it can be approximated by a plane wave $E = \exp[i\tilde{\phi}(x)]$. To interpret these results, let us consider the simple model where the phase $\tilde{\phi}$ is a normal random variable with mean $\langle\tilde{\phi}\rangle = 0$, variance $\sigma_\phi^2 \equiv \langle\tilde{\phi}^2\rangle$ and autocorrelation $\gamma_\phi(\xi) \equiv \langle\tilde{\phi}_1(x)\tilde{\phi}_2(x+\xi)\rangle/\sigma_\phi^2$. For the first two moments of the backward field we obtain $\langle E\rangle = \exp(-\sigma_\phi^2/2)$ and $\langle E_1 E_2^*\rangle = \exp[-\sigma_\phi^2(1-\gamma_\phi)]$, respectively, which are both decreasing functions of σ_ϕ. Consequently, in agreement with results in Fig. 2, as the level of fluctuations increases, the amplitude of the wave propagating along the direction of specular reflection (i.e. $\langle E\rangle$) decreases, and the spectrum of reflected waves (i.e. the Fourier transform of $\langle E_1 E_2^*\rangle$) broadens. In particular, for $\sigma_\phi \gg 1$, taking $\gamma_\phi(\xi) = \exp[-(\xi/\delta)^2]$ and expanding to the second order in ξ, we obtain $\langle E_1 E_2^*\rangle \approx \exp[-(\sigma_\phi\xi/\delta)^2]$. Thus, away from the cut-off, if Δk_x is the spectral width of fluctuations and $\sigma_\phi \Delta k_x \ll k_0$, the reflected waves will be distributed over the range of radial wavenumbers $\delta k_r \approx \sigma_\phi^2 \Delta k_x^2/2k_0$. Consequently, at a distance from $r = r_G$ larger than the diffraction distance $D = 1/\delta k_r$, the interference of waves will produce (as in Figs 1 and 3) a complicated field pattern with large amplitude variations and random phases. This suggests that the amplitude ρ of the measured signal must follow the distribution derived by Rice [7] for the case of a signal containing a sinusoidal coherent component and a Gaussian noise. It is given by

$$P(\rho) = \frac{\rho}{\sigma^2} e^{-(\rho^2+\rho_0^2)/2\sigma^2} I_0\Big(\frac{\rho\rho_0}{\sigma^2}\Big) \qquad (14)$$

where I_0 is the modified Bessel function of order zero, σ^2 is the variance of both the real and the imaginary parts of the Gaussian noise, and ρ_0 is the amplitude of the sinusoidal signal. Since in our numerical simulations the probing wave has unit amplitude, $\sigma^2 = (1-\rho_0^2)/2$ and $\rho_0^2 \approx \exp(-\sigma_\phi^2)$. For $\sigma_\phi \gg 1$, the Rice distribution becomes the Rayleigh distribution, in agreement with the experimental results of Fig. 1. A statistical analysis of several numerical realizations of E_b indicates that Eq. (14) is in very good agreement with our numerical results [5].

Obviously, this simple model of reflectometry must fail for large fluctuations. In fact, we can easily derive two conditions for its applicability. The first is given by the condition for the validity of 1-D geometric optics, which is $\Delta k_r < k_0/(k_0 L_\varepsilon)^{1/3}$ [3]. The second condition is imposed by the fact that, since each spectral component of the backward field originates near the corresponding reflecting point, our model of reflectometry must fail when these turning points are distributed over a distance Δr_c that is comparable to the radial scale length of fluctuations (Δk_r^{-1}), i.e. when $\Delta k_r \Delta r_c > 1$. Since for large fluctuations (i.e. $\sigma_\phi^2 \gg 1$) $\Delta r_c/L_\varepsilon \approx \sigma_\phi^2 \Delta k_x^2/k_0^2$, a second condition for the validity of our model is $\sigma_\phi^2 < k_0^2/L_\varepsilon \Delta k_r \Delta k_x^2$ [3]. For the ordinary mode of propagation, by expressing σ_ϕ^2 in terms of σ_n^2 (using Eqs (2)–(4)), this condition can be written in the form

$$\sigma_n^2 < \frac{1}{\pi^{3/2} L_n^2 \Delta k_x^2}. \qquad (15)$$

For the plasma parameters of Fig. 2 (where $L_n = 50$ cm), Eq. (15) gives $\sigma_n < 1.7 \times 10^{-2}$, which

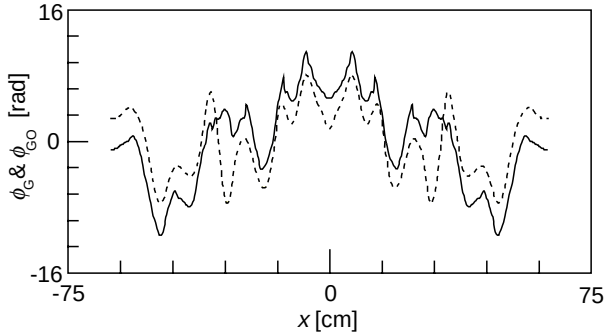

Figure 11. Fluctuating phases ϕ_G (solid line) and ϕ_{GO} (dashed line) for $\sigma_n = 2.0 \times 10^{-2}$ and other parameters as in Fig. 2.

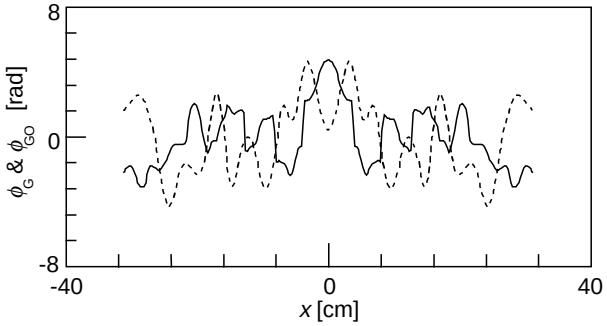

Figure 12. Fluctuating phases ϕ_G (solid line) and ϕ_{GO} (dashed line) for $\Delta k_x = 1$ cm^{-1} and other parameters as for case (c) in Fig. 6.

explains why we obtained $\phi_G \approx \phi_{GO}$ in all three cases of Fig. 6, where $\sigma_n \leq 1 \times 10^{-2}$. Finally, in the opposite limit of small fluctuations, where $\sigma_\phi^2 \ll 1$ and $\Delta r_c / L_\varepsilon \approx \Delta k_x^2 / k_0^2$, Eq. (15) becomes $\Delta k_x^2 \Delta k_r < k_0^2 / L_n$.

Figure 11 shows the result of doubling the value of σ_n ($= 2.0 \times 10^{-2}$) for case (c) of Fig. 6, making the amplitude of fluctuations larger than the limit imposed by Eq. (15). As expected, this results in a large discrepancy between ϕ_G and the phase of geometric optics ϕ_{GO}.

Another way of violating Eq. (15) is to increase the spectral width of plasma fluctuations. This is illustrated in Fig. 12, which shows the effect of doubling the value of Δk_x for case (c) of Fig. 6. Since this pushes the level of plasma fluctuations above the limit imposed by Eq. (15) ($\sigma_n = 0.8 \times 10^{-2}$), the result is again a large discrepancy between ϕ_G and ϕ_{GO}.

These results show how quickly ϕ_G departs from ϕ_{GO} when Eq. (15) is violated. In tokamaks, both theory and experiments indicate that the amplitude of short scale density fluctuations obeys the mixing length criterion $\sigma_n < 1/k_r L_n$ [1]. Hence Eq. (15) is automatically satisfied when $\Delta k_r > \pi^{3/4} \Delta k_x$.

5. Imaging reflectometry

The numerical results of the previous sections demonstrate that the spatial structure of density fluctuations near the cut-off could be obtained from the measurement of $\tilde{\phi}_G$. Such a measurement could be done by collecting the reflected waves with a wide aperture antenna, and by imaging the cut-off onto the detector plane taking the effect of the average plasma permittivity into account. This is the first novelty of the scheme proposed in this article. A second novelty is the simultaneous sampling of a large portion of a plasma magnetic surface, which requires the use of large microwave beams and of 2-D arrays of detectors. The latter are technically feasible, as shown in Ref. [8], which describes a microwave camera using a focal plane array (4 rows of 64 elements) for the measurement of the human body emission at 94 GHz with a resolution of 1 K and a frame rate of 30 Hz. Another example can be found in Ref. [9], which describes the measurement of the electron cyclotron emission in the TEXT tokamak using a wideband 20 channel Schottky diode array in the frequency range 90–110 GHz. More recently, similar measurements have been repeated in the RTP tokamak [10] using a 16 channel array in the range 100–140 GHz.

Figure 13 illustrates the conceptual design of a microwave imaging reflectometer for the visualization of plasma density fluctuations in tokamaks. In this scheme, as in the numerical simulations, the rays of the probing wave impinge perpendicularly upon the cut-off surface. This is obtained by using two cylindrical lenses (L_1 and L_2) with different focal points. For the case considered in Fig. 13, where the probing wave has a frequency of 120 GHz and the X mode of propagation, the focal point of L_2 is at $R = 2.3$ m, while obviously that of L_1 is at $R = 0$. Since the former depends on the wave frequency, the position of L_2 must be adjustable. Outside the plasma, then, the backward wave is reflected by the semitransparent reflector M, and an image of the cut-off is formed by the spherical lens L_3 onto the plane P, where the field is measured with a 2-D array of microwave receivers. In Fig. 13, it is also shown schematically how a local oscillator (LO) could be injected into the array from the back. Finally, by probing the plasma using simultaneously

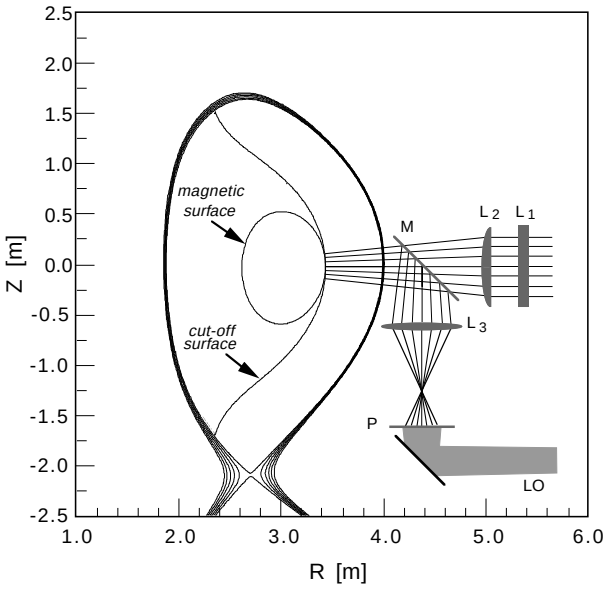

Figure 13. Conceptual design of an imaging reflectometer for a JET-like tokamak; L_1 and L_2 are cylindrical lenses, L_3 is a spherical lens, M is a semitransparent mirror and P is the detector plane. The shaded area on the bottom represents a local oscillator wave illuminating the detector array from the back.

multiple waves with closely spaced cut-offs, the proposed method could provide the full 3-D structure of plasma fluctuations.

In Fig. 13, the function of the cylindrical lenses L_1 and L_2 is to tailor the wave front of the probing wave to the shape of the cut-off surface, which is what allows the mapping of the cut-off surface onto the detector plane by the spherical lens L_3. Figures 14 and 15 show the results of replacing L_1 and L_2 with a single spherical lens optimizing the ray trajectories on either the poloidal (Fig. 14) or the toroidal (Fig. 15) plane. In both cases, L_3 would not be able to create an image of the reflecting cut-off onto the detector plane. Thus the use of L_1 and L_2 is to combine the poloidal ray trajectories in Fig. 14 with the equatorial trajectories in Fig. 15. Finally, to avoid the spurious effects of internal reflections inside refractive optical components, the optical scheme of Fig. 13 should be implemented using curved metallic mirrors.

The proposed method can use either the ordinary or the extraordinary mode of wave propagation, but the latter must be preferred because of the better spatial resolution that derives from the larger probing frequency of the extraordinary mode. The spatial resolution is given by $\delta \approx 2(\lambda_0/D)(r_b - r_G)$, where $\lambda_0 = 2\pi/k_0$ and D is the diameter of the probing beam. For the case of Fig. 13, we get $\delta \approx 1$ cm with $D = 50$ cm.

The proposed method could employ the same heterodyne detection techniques of standard reflectometry [3, 11], as illustrated by Fig. 16, which shows an example taken from Ref. [3] for a tunable system. In this block diagram, two local oscillators with frequencies f_1 and f_2 are used for producing a main signal (one for each array element) and a reference

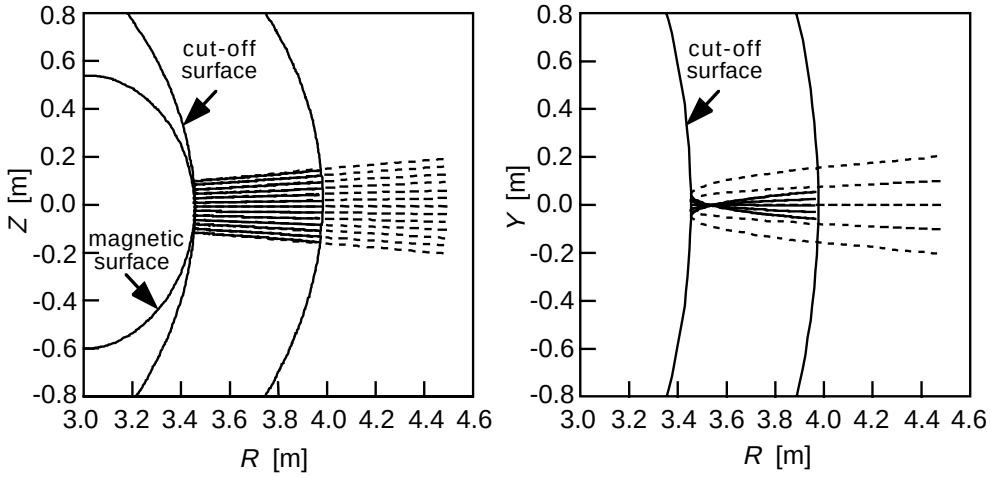

Figure 14. Ray trajectories (from a ray tracing code) of the probing wave in the absence of fluctuations when the focal length of L_1 in Fig. 13 is equal to that of L_2. Dashed lines represent the forward rays and solid lines the reflected rays on poloidal (left) and equatorial (right) planes.

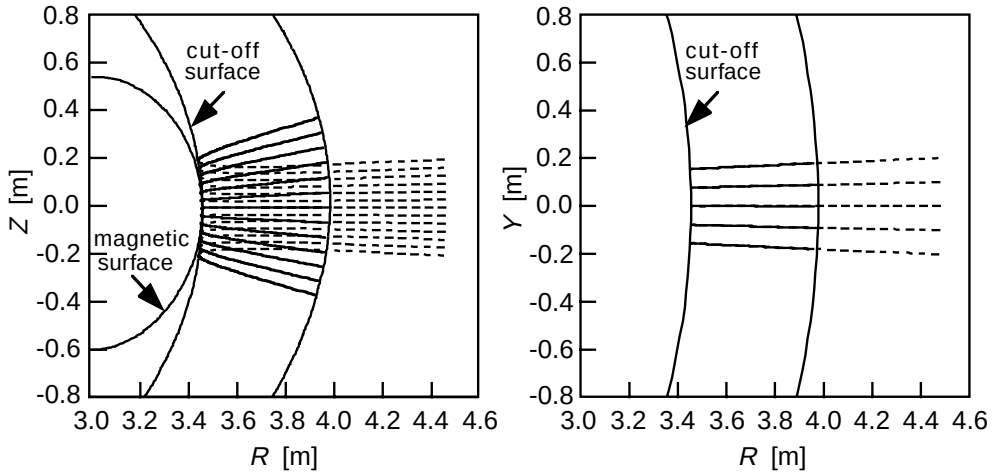

Figure 15. Same as in Fig. 13 when the focal length of L_2 in Fig. 13 is equal to that of L_1.

signal at the intermediate frequencies $f_2 - f_1 + f_r$ and $f_2 - f_1$, respectively (where f_r is the frequency of plasma fluctuations). As in standard reflectometry, this would then be followed by a final low frequency stage [3, 11] producing for each array element an in-phase and a quadrature component at frequency f_r.

Compared with standard reflectometry, the major difficulty in using heterodyne detection is represented by the amount of local oscillator (LO_1) power that is needed for driving the Schottky diode array. For instance, a 10×10 array would need at least 100 mW of LO power. Given the present availability of solid state millimetre wave sources, such as Gunn or IMPACT oscillators, this limits the use of imaging reflectometry to frequencies not much larger than 100 GHz. On the other hand, because of the very efficient way of collecting the reflected wave — a defining characteristic of imaging reflectometry — the probing wave does not need to be much larger than in standard reflectometry, where often the power losses inside the plasma are larger than 20 dB.

Another unique feature of the proposed method is the need for the acquisition and storage of a large number of signals. For example, for an imaging reflectometer with a 10×10 array and plasma fluctuations with a maximum frequency $f_r = 0.5$–1 MHz, it is necessary to acquire and store $(2$–$4) \times 10^8$ data s^{-1}. Fortunately, a complete characterization of the fast phenomena under investigation requires only a fraction of a second ($\leq$10 ms), which reduces the size of the problem considerably.

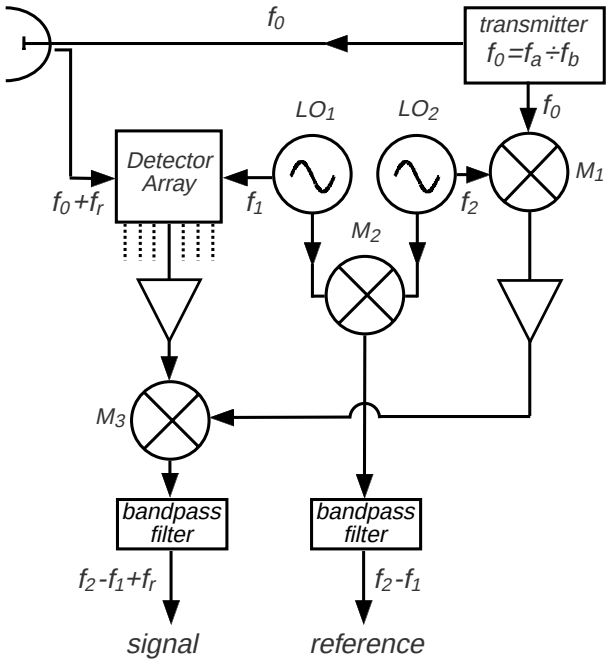

Figure 16. Block diagram of a tunable imaging reflectometer. LO_n: local oscillator; M_n: mixer. Each element of the detector array has a separate intermediate frequency stage comprising M_3.

6. Conclusion

In conclusion, the numerical results described in this article have clarified the role played by 2-D plasma fluctuations in microwave reflectometry. They indicate that, if the amplitude of fluctuations is below a threshold that is set by their spectrum of poloidal wavenumbers (Eq. (15)), it is possible to

obtain the local value of the density fluctuation by imaging the cut-off onto a detector plane. Indeed, this must be considered the only method for obtaining a localized measurement of 2-D plasma fluctuations with microwave reflectometry, regardless of whether the measurement is a single or a multipoint measurement.

The method of imaging reflectometry proposed in this article must be considered a first attempt at developing techniques for the global visualization of turbulent and coherent structures in tokamak plasmas. Undoubtedly its practical implementation presents serious difficulties, such as the need for large machine ports and 2-D arrays of microwave detectors. Nevertheless, this technique has the potential for providing new and important information on the spatial structure of turbulent fluctuations in tokamaks.

Acknowledgement

This work was supported by US Department of Energy contract DE-AC02-76-CHO-3073.

References

[1] Horton, W., Rev. Mod. Phys. **71** (1999) 735.
[2] Holmes, P.J., et al., Phys. Rep. **287** (1997) 337.
[3] Mazzucato, E., Rev. Sci. Instrum. **69** (1998) 2201.
[4] Mazzucato, E., et al., Phys. Rev. Lett. **77** (1996) 3145.
[5] Mazzucato, E., Rev. Sci. Instrum. **69** (1998) 1691.
[6] Mazzucato, E., Nazikian, R., Phys. Rev. Lett. **71** (1993) 1840.
[7] Rice, S.O., Bell Syst. Tech. J. **23** (1944) 282 and **24** (1945) 96 (reprinted in Wax, N., Selected Papers on Noise and Stochastic Processes, Dover, New York (1954)).
[8] Huguenin, G.C., SPIE **2938** (1996) 152.
[9] Hsia, R.P., et al., Rev. Sci. Instrum. **68** (1997) 488.
[10] Deng, B.H., et al., Rev. Sci. Instrum. **70** (1999) 998.
[11] Hartfuss, H.J., Geist, T., Hirsch, M., Plasma Phys. Control. Fusion **39** (1997) 1693.

(Manuscript received 19 March 2000
Final manuscript accepted 22 November 2000)

E-mail address of E. Mazzucato:
mazzucato@pppl.gov

Subject classification: D2, Te; K0, Te